Three-Dimensional FDTD Analysis of a Trapezoidal Antenna for Ultra Wideband Radio Applications

Sathaporn Promwong[†♦], Jun-ichi Takada[†], Pichaya Supanakoon[♦], Monchai Chamchoy[♦], Panarat Rawiwan[♦] and Prakit Tangtisanon[♦]

[†]Graduate School of Science and Engineering,
Tokyo Institute of Technology
2-12-1, O-okayama, Meguro-ku, Tokyo 152-8552, Japan.
E-mail: {ken,takada}@ap.ide.titech.ac.jp

[♦]Department of Information Engineering, Faculty of Engineering,
King Mongkut's Institute of Technology Lat Krabung, Bangkok 10520, Thailand.
E-mail: {kspichay,kcmoncha,krpanara,ktprakit}@kmitl.ac.th

Abstract

In this paper, a three-dimensianal (3-D) finite difference time domain (FDTD) method is used to analyze a trapezoidal antenna for ultra wideband (UWB) radio technology. The reflection coefficient ($|S_{11}|$) and voltage standing wave ratio (VSWR) are presented and compared with the measured results. The far field radiation pattern of this antenna is demonstrated. The far field frequency transfer function and impulse response of this antenna are shown. The distortion of the UWB pulse caused by this antenna is considered in the correlation coefficient term. The waveforms of UWB pulses which radiate at specific angles are shown. From the numerical results, we can see that this antenna is well matched and VSWR is less than 2:1 on frequency ranges from 3.1 to 10.6 GHz. The radiated field at the front of the antenna is vertically polarized The highest radiated power and lowest distortion of this antenna for UWB pulses are at about 60° from the front side of the antenna.

Keywords: Ultra wideband (UWB), finite difference time domain (FDTD), trapezodial antenna.

1. Introduction

Recently, ultra wideband (UWB) radio technology has becomes an important topic for microwave communication. UWB is different from other radio wave (RF) technology. Instead of using a narrow carrier frequency, UWB transmits pulses of power in the range of the ultra wide a frequency spectrum. The Federal Communication Commission (FCC) specifies that UWB has a frequency spectrum ranging from 3.1 to 10.6 GHz [1]. The power density of a UWB signal is considered to be noise for other communication systems because its power spectrum is below the noise level. The UWB receiver collects the power of the received signal to rebuilt the pulse. Therefore, UWB radio technology can exist with other RF technology without interference. UWB radio technology is an ideal candidate that can be utilized for commercial, short-range, low power, low cost indoor communication systems such as a wireless personal area network (WPAN) [2]-[4]

An antenna is an important part for the UWB radio technology. Conventional antennas are designed for use at only one frequency in general narrow band systems. If an impulse is excited on these antennas, the pulse will strongly distort and have time dispersion. An antenna for a nonsinusiodal wave has been proposed [5]-[6]. Next, a trapezoidal antenna was developed for an ultra wideband antenna [7]-[8].

In this paper, a three-dimensianal (3-D) finite difference time domain (FDTD) method is used to analyze a trapezoidal antenna for ultra wideband (UWB) radio technology. The antenna structure is considered as a one-port network. The impulse function is excited to evaluate

the frequency characeristics. The reflection coefficient ($|S_{11}|$) and voltage standing wave ratio (VSWR) are presented and compared with the measured results. The near electromagnetic fields are transformed to far electromagnetic fields. The far field radiation pattern of this antenna is demonstrated. The far field frequency transfer function and impulse response of this antenna are shown. The distortion of the UWB pulse caused by this antenna is considered in the correlation coefficient term. The UWB pulse is the Gaussian pulse with frequency ranging from 3.1 to 10.6 GHz. The waveforms of UWB pulses which radiate at the specific angle are shown. From the numerical results, we can see that this antenna is well matched and VSWR is less than 2:1 on frequency ranges from 3.1 to 10.6 GHz. The radiated field at the front of the antenna is vertically polarized. The highest radiated power and lowest distortion of this antenna for UWB pulses are at about 60° from the front side of the antenna.

2. FDTD Method

In this section, the FDTD algorithm for a trapezodial antenna analysis is described.

2.1 Finite Difference Equation

The finite difference equations are derived directly from Maxwell's curl equation in the time domain. Maxwell' curl equation of this problem can be written as:

$$\mu\frac{\partial\vec{H}}{\partial t}=-\nabla\vec{E}, \qquad (1)$$

$$\mu\frac{\partial\vec{E}}{\partial t}=\nabla\vec{H}. \qquad (2)$$

To obtain a discrete approximation of the continuous partial differential equations, the centered difference approximation is used on both the time and space first-order partial differences. The entire computation domain is the collection of all the unit cells. The dimensions of the unit cell along x, y and z directions are Δx, Δy and Δz, respectively. The node with subscript indices i, j and k corresponds to node number x, y and z directions. This notation implicitly assumes the $\pm 1/2$ space indices. The time steps are indicated with the superscript. After simple rearrangement, the finite difference equations are described below [9]:

$$H_x\big|_{i,j,k}^{n+1/2}=H_x\big|_{i,j,k}^{n-1/2}+\frac{\Delta t}{\mu}\left(\frac{E_y\big|_{i,j,k+1/2}^{n}-E_y\big|_{i,j,k-1/2}^{n}}{\Delta z}-\frac{E_z\big|_{i,j+1/2,k}^{n}-E_y\big|_{i,j-1/2,k}^{n}}{\Delta y}\right), \qquad (3)$$

$$H_y\big|_{i,j,k}^{n+1/2}=H_y\big|_{i,j,k}^{n-1/2}+\frac{\Delta t}{\mu}\left(\frac{E_z\big|_{i+1/2,j,k}^{n}-E_z\big|_{i-1/2,j,k}^{n}}{\Delta x}-\frac{E_x\big|_{i,j,k+1/2}^{n}-E_x\big|_{i,j,k-1/2}^{n}}{\Delta z}\right), \qquad (4)$$

$$H_z\big|_{i,j,k}^{n+1/2}=H_z\big|_{i,j,k}^{n-1/2}+\frac{\Delta t}{\mu}\left(\frac{E_x\big|_{i,j+1/2,k}^{n}-E_x\big|_{i,j-1/2,k}^{n}}{\Delta y}-\frac{E_y\big|_{i+1/2,j,k}^{n}-E_y\big|_{i-1/2,j,k}^{n}}{\Delta x}\right), \qquad (5)$$

$$E_x\big|_{i,j,k}^{n+1}=E_x\big|_{i,j,k}^{n}+\frac{\Delta t}{\varepsilon}\left(\frac{H_z\big|_{i,j+1/2,k}^{n+1/2}-H_z\big|_{i,j-1/2,k}^{n+1/2}}{\Delta y}-\frac{H_y\big|_{i,j,k+1/2}^{n+1/2}-H_y\big|_{i,j,k-1/2}^{n+1/2}}{\Delta z}\right), \qquad (6)$$

$$E_y\big|_{i,j,k}^{n+1}=E_y\big|_{i,j,k}^{n}+\frac{\Delta t}{\varepsilon}\left(\frac{H_x\big|_{i,j,k+1/2}^{n+1/2}-H_x\big|_{i,j,k-1/2}^{n+1/2}}{\Delta z}-\frac{H_z\big|_{i+1/2,j,k}^{n+1/2}-H_z\big|_{i-1/2,j,k}^{n+1/2}}{\Delta x}\right), \qquad (7)$$

$$E_z\Big|_{i,j,k}^{n+1} = E_z\Big|_{i,j,k}^{n} + \frac{\Delta t}{\varepsilon}\left(\frac{H_y\Big|_{i+1/2,j,k}^{n+1/2} - H_y\Big|_{i-1/2,j,k}^{n+1/2}}{\Delta x} - \frac{H_x\Big|_{i,j+1/2,k}^{n+1/2} - H_x\Big|_{i,j-1/2,k}^{n+1/2}}{\Delta y} \right), \quad (8)$$

where ε and μ are the free space permittivity and permeability, respectively.

The half time steps indicate that E and H are calculated alternately.

The maximum time step is limited by the stability restriction of finite difference equation [10]:

$$\Delta t = \frac{1}{c}\sqrt{\frac{1}{\Delta x^2} + \frac{1}{\Delta y^2} + \frac{1}{\Delta z^2}}, \quad (9)$$

where c is the velocity of the light in free space.

2.2 Resistive Voltage Source Model

A voltage source V_s is presented as an electric field E in the y direction at the node i_s, j_s and k_s along x, y and z axis, respectively. If the source resistance is set to R_s, then the usual FDTD electric field at the source location is given by [11]:

$$E_y\Big|_{i_s,j_s,k_s}^{n+1} = \frac{1}{\Delta z} V_s\Big|^{n+1} + \frac{R_s}{\Delta z} I_s\Big|^{n+1/2}, \quad (10)$$

when the current through the source is given by:

$$I_s\Big|^{n+1/2} = \frac{H_x\Big|_{i_s,j_s,k_s+1/2}^{n+1/2} - H_x\Big|_{i_s,j_s,k_s-1/2}^{n+1/2}}{\Delta z} - \frac{H_z\Big|_{i_s+1/2,j_s,k_s}^{n+1/2} - H_z\Big|_{i_s-1/2,j_s,k_s}^{n+1/2}}{\Delta x}. \quad (11)$$

This resistive voltage source model is used to consider the antenna as a one-port network and to excite the voltage signal to the antenna.

2.3 PML ABC Treatment

The tangential field components on all six mesh walls must be specified in such a way that outgoing waves are not reflected. In this paper, a perfectly matched layer absorbing boundary condition (PML ABC) [12] is used.

The PML ABC can absorb propagation waves effectively by using nonphysical lossy media adjacent to the outer-grid boundaries backed by perfectly conducting walls. Based on the splitting of the field components into two subcomponents, the electric loss σ and magnetic loss σ^* for a PML medium are specified by satisfying the PML impedance-matching condition:

$$\frac{\sigma}{\varepsilon} = \frac{\sigma^*}{\mu}. \quad (12)$$

After the introduction of electric and magnetic losses, electromagnetic waves inside a PML medium will attenuate rapidly and explicit exponentially differenced field-updating equations are used to replace the conventional FDTD algorithm.

The electric loss in the PML region is assumed to increase with depth from zero at $\rho = 0$ to a maximum value of $\sigma_{\max}$ at $\rho = \delta$ by the quadratic ramping:

$$\sigma(x) = \sigma_{\max}\left(\frac{\rho}{\delta}\right)^2, \quad (13)$$

where $\sigma_{\max}$ is chosen to bound the PML reflection coefficient. The PML reflection coefficient at normal incident $R(0)$ has the following expression:

$$R(0) = \exp\left(\frac{-2\varsigma_{\max}\delta}{3c\varepsilon}\right). \quad (14)$$

2.4 Near to Far Field Transformation

For the electromagnetic analysis by using FDTD method, the provided data are near field. Therefore, these near field data are transformed to the far field data. Then, the far field data are used to calculate the radiation pattern, far field transfer function and impulse response.

First, we will consider the frequency domain. Let us assume that the analyzed antenna is enclosed by the close surface S'. Further, assume that this close surface has the local unit outward normal vector $\hat{n}$. Then, the electric and magnetic current densities, $\vec{J}_s(\omega)$ and $\vec{M}_s(\omega)$ can be written as:

$$\vec{J}_s(\omega) = \hat{n} \times \vec{H}(\omega), \quad (15)$$

$$\vec{M}_s(\omega) = -\hat{n} \times \vec{H}(\omega), \quad (16)$$

where $\vec{E}(\omega)$ and $\vec{H}(\omega)$ are electric and magnetic fields that propagate on the surface.

Later, we can define the time harmonic vector potential $\vec{N}(\omega)$ and $\vec{L}(\omega)$ [13]:

$$\vec{N}(\omega) = \int_{S'} \vec{J}_s(\omega) e^{jk\vec{r}'\cdot\hat{r}} dS', \quad (17)$$

$$\vec{L}(\omega) = \int_{S'} \vec{M}_s(\omega) e^{jk\vec{r}'\cdot\hat{r}} dS', \quad (18)$$

where $j = \sqrt{-1}$, k is the wave number, $\hat{r}$ is the unit vector to the far field point and $\vec{r}$ is the vector to the source point of integration.

In order to develop the corresponding time domain far field transformation, we need to take the inverse Fourier transforms of the above equations. There is frequency dependence in above equation. To simplify the inverse Fourier transformation process, we first define time harmonic vector potentials $\vec{W}(\omega)$ and $\vec{U}(\omega)$:

$$\vec{W}(\omega) = \frac{j\omega\vec{N}(\omega)}{4\pi rc} e^{-j\omega r/c}, \quad (19)$$

$$\vec{U}(\omega) = \frac{j\omega\vec{N}(\omega)}{4\pi rc} e^{-j\omega r/c}, \quad (20)$$

where r is the distance from the origin to the far field point.

Next, we recognize that the $j\omega$ multiplier in previous equations corresponds to a time derivative and the exponential factors containing $j\omega$ correspond to the time shifts. Thus, we can readily take inverse transforms $\vec{W}(\omega)$ and $\vec{U}(\omega)$ to obtain the time domain vector potentials:

$$\vec{W}(t) = \frac{\partial}{\partial t} \int_{S'} \left\{ \frac{\vec{J}_s\left(t - \frac{r - \vec{r}'\cdot\hat{r}}{c}\right)}{4\pi rc} \right\} dS', \quad (21)$$

$$\vec{U}(t) = \frac{\partial}{\partial t} \int_{S'} \left\{ \frac{\vec{M}_s\left(t - \frac{r - \vec{r}'\cdot\hat{r}}{c}\right)}{4\pi rc} \right\} dS'. \quad (22)$$

These vector potentials are in the Cartesian coordinate system. Next, these vector potentials are converted to the spherical coordinate system:

$$W_\theta(t) = W_x(t)\cos\theta\cos\phi + W_y(t)\cos\theta\sin\phi + W_z(t)\sin\theta, \quad (23)$$

$$W_\phi(t) + W_y(t)\cos\phi - W_x(t)\sin\phi, \quad (24)$$

$$U_\theta(t) = U_x(t)\cos\theta\cos\phi + U_y(t)\cos\theta\sin\phi + U_z(t)\sin\theta, \quad (25)$$

$$U_\phi(t) + U_y(t)\cos\phi - U_x(t)\sin\phi. \quad (26)$$

Finally, the far field electric field can be calculated by [14]:

$$E_\theta(t) = -\eta W_\theta(t) - U_\phi(t) \quad (27)$$

$$E_\phi(t) = -\eta W_\phi(t) - U_\theta(t) \quad (28)$$

where η is the intrinsic impedance of free space.

3. Numerical Results

The trapezoidal antenna is used to analyze the antenna characteristics and consider the distortion of a UWB pulse. The structure and dimensions of this antenna are shown in figure 1.

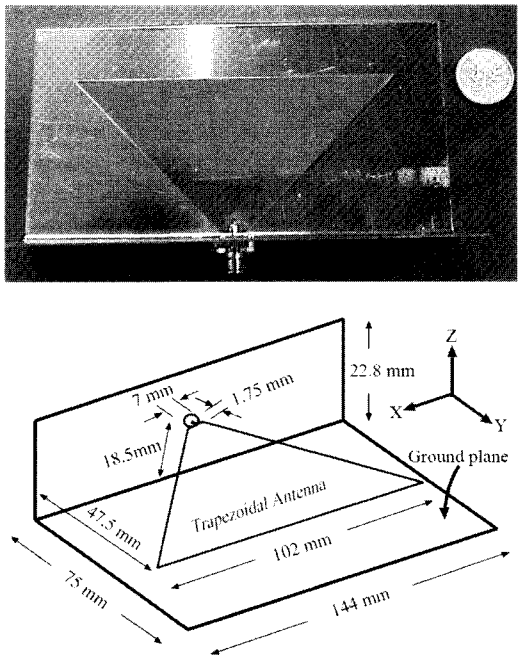

Fig. 1. Structure and dimensions of Trapezoid antenna.

For the FDTD simulation, the cell dimension along x, y and z are Δx=1.4496 mm, Δy=1.4412 mm and Δz=1.4270 mm, respectively. The entire calculation domain including the PML medium is $136\times89\times53$ cells. The interval of each time step is $\Delta t = 2.7716$ ps and uses 2,000 time steps for this simulation. The PML medium is set to 8 layers. The reflection coefficient at the normal incident is $R(0)=10^{-15}$. The distance from the origin to the far field, for the near to far field transformation, is set to be $r = 9.8021$ cm.

For the excitation, the resistive voltage source model is used. The internal resister is set to be $R_s = 50\ \Omega$. For the analyzing of the antenna characteristics, the estimated impulse voltage source is used:

$$V_s = \begin{cases} \dfrac{1}{\Delta t} & \text{for} \quad n=0 \\ 0 & \text{for elsewhere} \end{cases}, \qquad (29)$$

where n is the time step. This equation is an impulse function with frequency ranges from DC to infinity. The graph of this function is estimated to be a triangle as shown in figure 2. Then, its value at $n=0$ is $1/\Delta t$ when normalizing the area to 1.

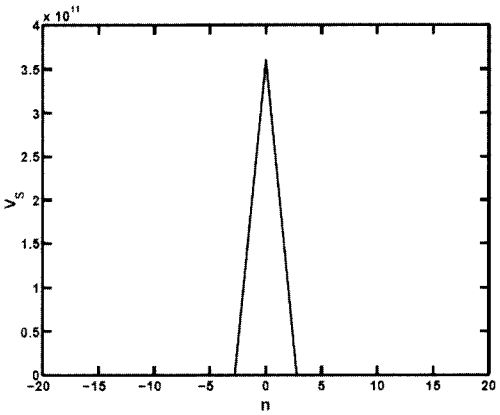

Fig. 2. Impulse voltage is estimated as a triangular function

Figure 3 shows the reflection coefficient ($|S_{21}|$) which can be obtained from FDTD simulation and comparing with measurements results. From this figure, we can see that most of the value of the $|S_{21}|$ parameter obtained from both FDTD simulation and measured result are below -10 dB in the range from 3.1 to 10.6 GHz.

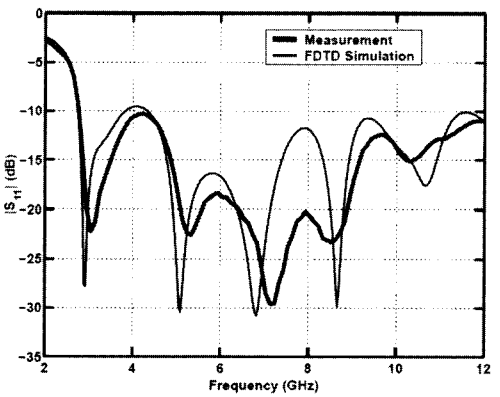

Fig. 3. $|S_{21}|$ parameter obtained form FDTD simulation compared with that obtained from measured result.

The VSWR parameter obtained from FDTD simulation, when compared with that from measured result, is shown in figure 4. From this figure, we can see that the VSWR parameter is less than 2:1 in the range from 3.1 to 10.6 GHz. Therefore, this antenna has low reflection loss

and good impedance matching in the desired frequency range from 3.1 to 10.6 GHz.

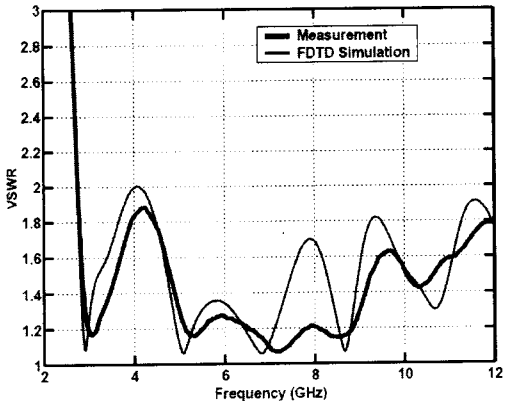

Fig. 4. VSWR parameter obtained from FDTD simulation compared with that obtained from measured result.

Figures 5 and 6 show the magnitude and phase of the far field frequency transfer function at the front side of the antenna. From these figures, we can see that the magnitude of the radiated field is highly attenuated at frequencies of 6.4, 8.0, 6.1 and 10.6 GHz. At these frequencies, the phase of the radiated field is also nonlinear.

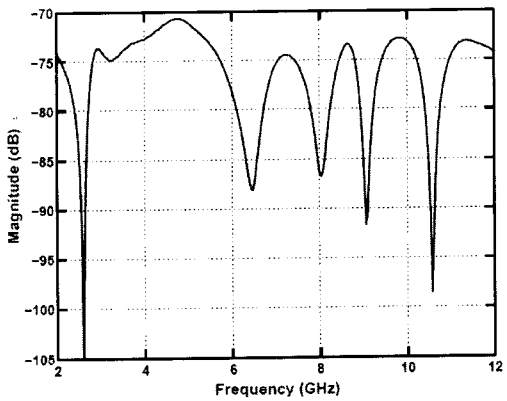

Fig. 5. Magnitude of far field frequency transfer function at the front side of the antenna.

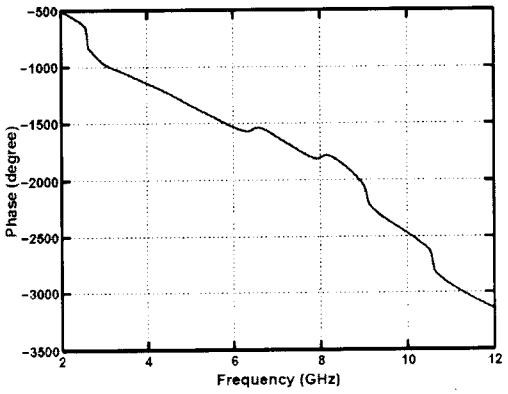

Fig. 6. Phase of far field frequency transfer function at the front side of the antenna.

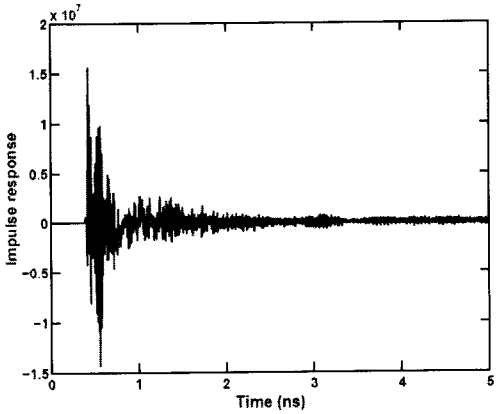

Fig. 7. Far field impulse response at the front side of the antenna.

The far field impulse response at the front side of the antenna is shown in figure 7. We can use this parameter to find the radiated field via the convolution of the specific voltage source with this far field impulse response.

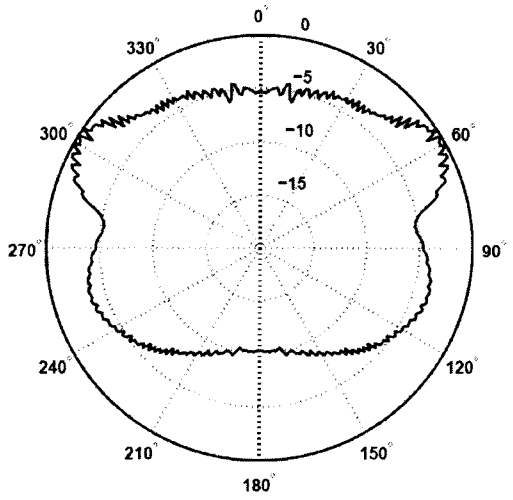

Fig. 8. Radiation pattern of E_θ.

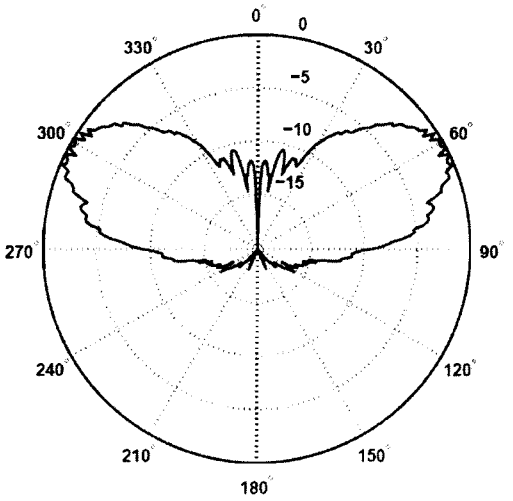

Fig. 9. Radiation pattern of E_ϕ.

For the UWB antenna, the radiation pattern is considered from the maximum absolute value of far field impulse response that radiates at any direction. In this paper, the radiation patterns in the horizontal plane (xy plane) are considered. The radiation patterns of E_θ (vertical polarization) and E_ϕ (horizontal polarization) are shown in figures 8 and 9, respectively. From these figures, we can see that the waves radiating at the front side of the antenna have vertical polarization and the highest radiated wave is at about 60° from the front side of the antenna.

For considering the distortion caused by this antenna, the pulse was a Gaussian UWB pulse with the frequency f_c at 6.85 GHz and its equation is [14]:

$$v_t(t) = v_0 e^{-[(t-t_c)/t_d]^2} \sin(2\pi f_c t). \quad (30)$$

This pulse is centered at time step t_c and has a $1/e$ characteristic decay of t_d. The parameter t_c is set to be $3/(2f_c)$ for the pulse, which has zero DC component. The three UWB pulse waveforms, which have 50, 70 and 90 percent of the average power in the frequency range from 3.1 to 10.6 GHz, are considered. For the 50, 70 and 90 percent of the average power, the parameter t_d is set to be 2.6616×10^{-11}, 3.7730×10^{-11} and 6.8188×10^{-11}, respectively. These UWB pulses are normalized by coefficient v_0 and set to be 3.5300×10^5, 2.4030×10^5 and 1.5402×10^5 for the pulse with 50, 70 and 90 percent of the average power, respectively. These UWB pulse waveforms are shown in figure 10.

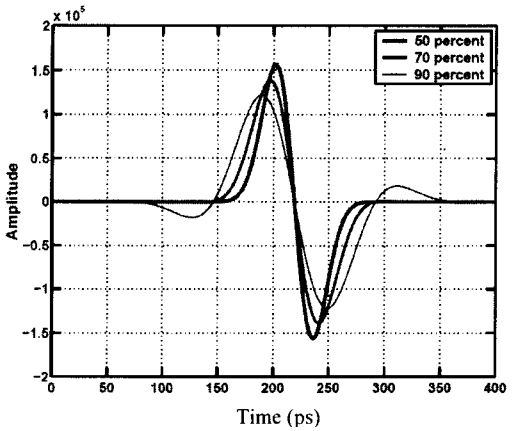

Fig. 10 UWB pulse waveforms which have 50, 70 and 90 percent of the average power in the frequency range from 3.1 to 10.6 GHz.

The radiated waveforms of these UWB pulses from the trapezoidal antenna at the front, left or right and back sides are investigated. Figures 11 to 13 show the radiated waveform from these UWB pulses at the front, left or right and bank sides, respectively. From these figures, we can seen that the radiated waveforms which have 50, 70 and 90 percent of the average power in the frequency range from 3.1 to 10.6 GHz,

almost have similar shapes. For these cases, the maximum amplitude is radiated from the left or right sides while the minimum amplitude is radiated from the back side of the antenna. The radiated pulse at the left or right sides have reflected pulses which are less than the front and back sides.

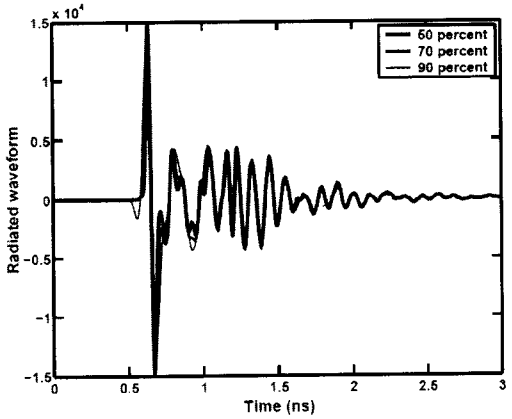

Fig. 11 Radiated waveforms which have 50, 70 and 90 percent of average power in the frequency range from 3.1 to 10.6 GHz at the front side of the trapezoidal antenna.

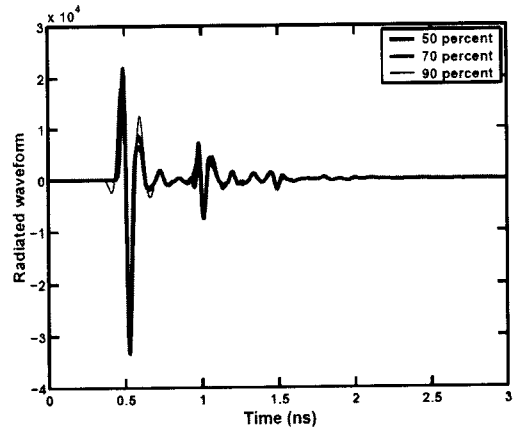

Fig. 12 Radiated waveforms which have 50, 70 and 90 percent of average power in the frequency range from 3.1 to 10.6 GHz at the left or right side of the trapezoidal antenna.

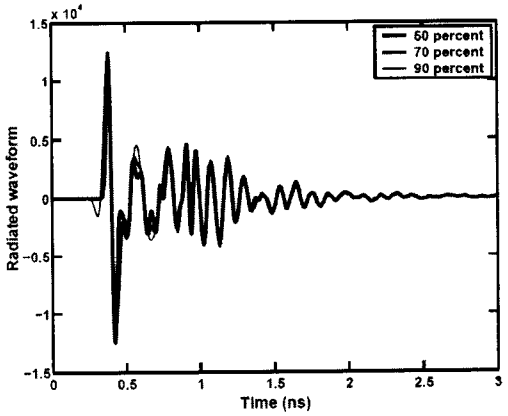

Fig. 13 Radiated waveforms which have 50, 70 and 90 percent of average power in the frequency range from 3.1 to 10.6 GHz at the back side of the trapezoidal antenna.

For the distortion quantity of the pulse waveform, we consider the correlation coefficient of the UWB pulse and radiated pulse waveform at an arbitrary angle. The correlation coefficients of these UWB pulses at the arbitrary angle of the trapezoidal antenna are shown in figure 14. From this figure, we can see that the correlation coefficients of all three cases are more than 0.7. The peak of correlation coefficient values are at $\pm 20°$, $\pm 65°$, $\pm 115°$ and $\pm 160°$. The distortion of the UWB pulse, which has 50 percent of the average power, is less than the 70 and 90 percent of the average power in the frequency range from 3.1 to 10.6 GHz

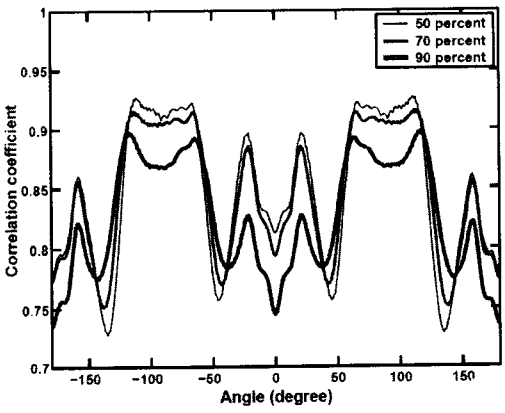

Fig. 14 Correlation coefficients of the UWB waveforms at the arbitrary angle of the trapezoidal antenna.

4. Conclusion

In this paper, a three-dimensianal (3-D) finite difference time domain (FDTD) method is used to analyze trapezoidal antenna for ultra wideband (UWB) radio technology. The distortion of the UWB pulse caused by this antenna is considered in the correlation coefficient term. From the numerical results, we can see that this antenna is well matched and VSWR is less than 2:1 on frequency ranges from 3.1 to 10.6 GHz. The radiated field at the front of the antenna is vertically polarized. The highest radiated power and lowest distortion of this antenna for UWB pulse are at about 60° from the front side of the antenna. The disadvantage of this trapezoidal antenna is that the best radiated wave and the correlation coefficient are not at the front side of the antenna.

5. References

[1] Federal Communications Commission, Revision of Part 15 of the Commission's Rules Regarding Ultra-Wideband Transmission Systems, First Report and Order, FCC 02–48, Apr. 2002.

[2] K. Siwiak, Ultra-Wide Radio: Introduccing a New Technology, 2001 Spring IEEE Veh. Tech. Conf. (VTC), Plenary session, pp.1088-1093, May 2001.

[3] K. Siwiak, Ultra-Wide Radio: The emergence of an Important RF Technology, Proc. 2001 Spring IEEE Veh. Tech. Conf. (VTC), pp.1169-1172, May 2001.

[4] J. Farserotu, A. Hutter, F. Platbrood, J. Gerrits, A. Pollini, UWB Transmission and MIMO Antenna Systems for Nomadic User and Mobile PAN, Wireless Personal Commun., No.22, pp.197-317, 2002.

[5] H.F. Harmuth and S. Ding-Rong, Antennas for Nonsinusiodal Wave-Part I: Radiators, IEEE Trans. Elec. Mag. Compat., Vol.EMC-25, No.1, pp.13-24, Feb. 1983.

[6] H.F. Harmuth and S. Ding-Rong, Antennas for Nonsinusiodal Wave-Part II: Sensors, IEEE Trans. on Elec. Mag. Compat., Vol.EMC-25, No. 1, No. 2, pp. 107-115, May 1983.

[7] A. Duzdar and G. Kompa, A Novel Trapesoidal Antenna Fed by A Ground Image Plane and Backed by a Reflector, Proc. Euro. Microwave Workshop (EuMC) 2000, Vol.2, pp.1-4, Paris, France, Sept. 2000.

[8] S. Promwong, W. Hachitani, and J. Takada, Experimental Evaluation Scheme of UWB Antenna Performance, IEEJ. IM 2003-29-35, pp.37-42, Sagamihara, Kanagawa, June 2003.

[9] K. S. Yee, Numerical Solution of Initial Boundary Value Problems Involving Maxwell's Equations in Isotropic Media, IEEE Tran. Antennas Propagat., Vol. AP-14, pp.302-307, 1966.

[10] A. Taflove and M. E. Brodwin, Numerical Solution of Steady-State Electromagnetic Scattering Problems Using The Time-Dependent Maxwell's equation, IEEE Trans. Microwave Theory Tech., Vol.23, pp.623-630, 1975.

[11] R. J. Luebbers and H. S. Langdon, A Simple Feed Model Reduces Time Steps Needed for FDTD Antenna and Microstrip Calculations, IEEE Trans. Antennas Propagat., Vol.44, No.7, pp. 1000-1005, 1996.

[12] J. P. Berenger, A Perfectly Matched Layer for the Absorption of Electromagnetic Waves, J. Computational Physics, Vol. 144, pp.185-200, 1994.

[13] S. Ramo, J. Whinnery and T. Van Duzer, Fields and Waves in Communication Electronics, 2nd ed., John Wiley & Sons, New York, 1984.

[14] S. Promwong, J. Takada, P. Supanakoon, M. Chamchoy, A. Pradabphon and P. Tangtisanon, Distortion Analysis of UWB Pulse Caused by Trapezoidal Antenna, 26th Electrical Engineering Conference (EECON 26), pp.1494-1499, Nov 2003.